Research Square

Preprints are preliminary reports that have not undergone peer review.
They should not be considered conclusive, used to inform clinical practice,
or referenced by the media as validated information.

Histone H3S28 Phosphorylation Promotes a Senescence-Associated Survival Program Following PARP Inhibition in Hormone Receptor-Positive Breast Cancer

Anna Tomàs Pujolà
Universitat Internacional de Catalunya
Evangelos Manousakis
Universitat Internacional de Catalunya
Clàudia Martinez Miralles
Universitat Internacional de Catalunya
Houda Baccara
University of Parma
Laia Liñán Franquet
Universitat Internacional de Catalunya
Roberto Ferrari
University of Parma
Cristina Moreta-Moraleda
cmoreta@uic.es
Universitat Internacional de Catalunya
Roni H. G. Wright
Universitat Internacional de Catalunya

Research Article

Keywords: Breast cancer, Poly ADP-Ribose polymerase 1 (PARP1), Histone 3 serine 28 phosphorylation (H3S28ph), PARPi resistance, Olaparib, DNA damage, Senescence

Posted Date: August 6th, 2026

DOI: https://doi.org/10.21203/rs.3.rs-10431382/v1

License: This work is licensed under a Creative Commons Attribution 4.0 International License.
Read Full License

Additional Declarations: No competing interests reported.

Abstract

Background:

PARP1 inhibitors (PARPi) are a key therapeutic strategy in BRCA1/2-mutated and increasingly in homologous recombination (HR)-positive breast cancers. However, resistance and relapse remain major challenges. While most studies focus on DNA repair restoration, chromatin-based mechanisms of PARPi response are less understood. PARP1 regulates DNA repair and chromatin organisation through poly(ADP-ribosyl)ation and histone modification. Histone H3 serine 28 phosphorylation (H3S28ph), a stress- and DNA damage-responsive mark catalysed by MSK1/2, is associated with chromatin relaxation and senescence. We hypothesised that H3S28ph promotes a senescence-associated survival programme contributing to PARPi resistance in HR-positive breast cancer.

Methods:

HR-positive breast cancer cell lines were exposed to UV-induced DNA damage and treated with the PARP inhibitor olaparib. H3S28 phosphorylation dynamics were assessed by immunofluorescence, Western blotting and chromatin immunoprecipitation. Functional effects were evaluated using proliferation, clonogenic growth, spheroid formation and cell cycle analysis. Senescence was quantified by β-galactosidase staining and expression of senescence-associated genes by RT-qPCR. Clinical relevance was assessed using Kaplan–Meier Plotter, GEPIA3, and the GSE173839 cohort.

Results:

DNA damage induced robust H3S28 phosphorylation, which was enhanced by PARP inhibition. H3S28ph was enriched at promoters of senescence-associated genes, including *CDKN2A* (p14/p16), *CDKN2B* (p15) and FOXA1, leading to their transcriptional activation. Combined UV and PARPi treatment induced G1/S arrest, increased senescence markers and enhanced β-galactosidase activity, consistent with a therapy-induced senescence-like state. Clinically, low expression of MSK1 (*RPS6KA5*) and associated senescence genes correlated with poorer overall survival and differential response to DNA-damaging therapies in HR-positive breast cancer cohorts.

Conclusions:

Our findings indicate that H3S28 phosphorylation acts as a chromatin-based adaptive mechanism linking DNA damage signalling to senescence-associated transcription under PARP inhibition. The MSK1–H3S28ph axis promotes a senescence-like survival state that may contribute to PARPi resistance in HR-positive breast cancer. Targeting this epigenetic pathway may improve therapeutic response and overcome resistance.

Background

Poly(ADP-ribose) polymerase 1 (PARP1) inhibitors (PARPi) have reshaped the treatment landscape for breast cancer, particularly in tumours with BRCA1 or BRCA2 mutations where homologous recombination (HR) repair is defective. Yet their use is now expanding beyond this original setting. Increasing evidence suggests that a subset of HR-positive (HR^+) breast cancers also display features of HR deficiency and may benefit from PARPi therapy. For instance, recent clinical studies have reported improved pathological complete response rates when PARPi are added to neoadjuvant regimens in both HR-positive and HR-negative subtypes [1–3]. Despite these promising results, resistance to PARPi remains a major clinical challenge: between 40% and 70% of patients eventually relapse after an initial response, underscoring the need to identify new mechanisms of resistance and markers predictive of treatment failure.

Most known resistance mechanisms involve restoration of HR function, stabilization of replication forks, or altered drug efflux [4, 5]. However, these processes do not fully explain the frequency and diversity of resistance observed clinically, therefore increasing attention is turning to the chromatin context in which PARP1 operates.

PARP1 plays a central role in the DNA damage response (DDR) by catalysing poly(ADP-ribosyl)ation (PARylation) of itself and chromatin-associated proteins to facilitate chromatin relaxation and recruitment of DNA repair machinery [6–8]. Beyond its canonical repair functions, PARP1 contributes to chromatin remodelling and gene regulation through multiple mechanisms. These include direct PARylation of histone tails to modulate chromatin accessibility, participation in nuclear ATP synthesis required for chromatin remodelling, resolution of R-loops to maintain transcriptional integrity, and the formation of nuclear condensates via phase separation to spatially coordinate transcriptional programs [9, 10]. Because of this multifaceted chromatin-associated activity, PARP1 is considered a master regulator of genome organization and transcriptional control [11].

Indeed, cells that survive PARP1 inhibition often undergo profound epigenomic reprogramming, activating alternative survival pathways to bypass PARP1 dependency. Several studies from our group and others have demonstrated that PARP1 not only functions in DNA repair but also mediates hormone-dependent transcription in breast cancer cells [7, 12–14]. These findings reinforce the view of PARP1 as a chromatin-based transcriptional regulator and suggest that chromatin dynamics could compensate for the loss of PARP1 activity. Deciphering these compensatory pathways may reveal key vulnerabilities in resistant breast cancer cells and inform new therapeutic strategies.

One modification of particular interest is phosphorylation of histone H3 at serine 28 (H3S28ph). This epigenetic mark is rapidly induced by mitogen- and stress-activated kinases MSK1/2, which act downstream of the ERK and p38 MAPK pathways. H3S28 phosphorylation is known to loosen local chromatin structure, affecting the binding of transcription factors and activating immediate-early gene transcription [15, 16]. Under persistent stress or DNA damage, it has also been linked to the onset of cellular senescence—a state of permanent growth arrest accompanied by metabolic and transcriptional changes. Indeed, H3S28 phosphorylation facilitates the displacement of Polycomb repressive complex 2

(PRC2) required for the induction of senescence via the activation of INK4AB/ARF genes [17]. While senescence can act as a tumour-suppressive barrier, senescent tumour cells may also survive therapy and drive relapse through secretion of pro-inflammatory and pro-tumorigenic factors, collectively termed the senescence-associated secretory phenotype (SASP).

Given that both PARP1 and H3S28ph respond to DNA damage and influence chromatin accessibility, we hypothesised that H3S28 phosphorylation might alter the chromatin environment during PARPi treatment, tipping the balance between apoptosis and senescence. In HR$^+$ breast cancer, where residual DNA repair capacity and hormonal signalling may favour survival under genotoxic stress, this mechanism could be particularly relevant.

In this study, we examined how DNA damage and PARPi exposure interact to regulate H3S28 phosphorylation, cell survival, and senescence in HR$^+$ breast cancer cell lines. We used ultraviolet (UV) irradiation to model DNA-damage-induced stress and assessed clonogenic growth, spheroid formation, and senescence-associated gene expression following PARPi treatment. Finally, to evaluate clinical relevance, we analysed patient cohorts for expression of MSK1—the upstream kinase responsible for H3S28 phosphorylation—and p15, a senescence marker previously linked to H3S28ph regulation. Together, our findings reveal a potential chromatin-based mechanism that allows breast cancer cells to survive PARPi exposure, identifying the H3S28ph–MSK1 axis as a promising biomarker of resistance and relapse in HR-positive breast cancer.

Methods

Cell culture

Human HR$^+$ breast cancer cell lines BT474 and MCF7 were obtained from the American Type Culture Collection (ATCC) and cultured in adherent conditions (2D) and non-adherent conditions (3D). For 2D cultures, cells were cultured in DMEM (Sigma-Aldrich, Cat. D5671) supplemented with 10% fetal bovine serum (FBS), 1% penicillin/streptomycin (P/S), and 1% L-Glutamine. For 3D cultures, cells were cultured in DMEM-F12 (Sigma-Aldrich, Cat. D8437) supplemented with 10% FBS, 1% P/S, 1% L-Glutamine, 2% B-27, and 20 ng/ml epidermal growth factor (EGF). All cell lines were incubated at 37°C with 5% CO_2.

UV irradiation

To induce UV-mediated damage in BT474 and MCF7 cell lines, culture medium was removed from the plates prior to irradiation. Cells were exposed to the indicated UV dose (J/cm^2) using a Vilber Lourmat UV Crosslinker BLX 254. Following irradiation, the original culture medium was returned to the plates, which were subsequently incubated at 37°C with 5% CO_2 until further processing.

Protein extraction and quantification

Cells were lysed in lysis buffer (0.5% NP-40, 150 mM NaCl, 50 mM Tris HCl (pH 8.0) and 1X Complete™ Protease Inhibitors Cocktail without EDTA (Cat. 05056489001, Roche) for 30 minutes (min) on ice. Lysates were centrifuged at 12.000 rpm for 15 minutes at 4 ºC to remove insoluble material. Protein quantification was determined using the Pierce™ BCA Protein Assay kit (ThermoFisher Scientific, Cat. 23225) following manufacturer's protocol.

Western blotting

Equal amounts of protein (20 µg) were separated using Tris-Glycine Precast Gels (4–15%; Bio-Rad, Cat. 4561083) and transferred into nitrocellulose membranes (0.45 µm, Bio-rad, Cat.1620115). After blocking with 5% non-fat milk in TBS-T (TBS containing 0.05% Tween-20) for 1 hour (h) at room temperature (RT), membranes were incubated overnight at 4°C with primary antibodies against H3S28ph (1:1000; Cell Signalling, Cat. 9713), PAR/pADPr (1:1000; R&D Systems, Cat. 4335-MC-100) and GAPDH (1:1000, Santa Cruz Biotechnology, Cat. sc365062). Following three washes with TBS-T, membranes were incubated with secondary antibodies (goat anti-mouse IgG, 1:10.000; Jackson ImmunoResearch, Cat. 515-035-003; and goat anti-rabbit IgG, 1:10.000; Jackson ImmunoResearch, Cat. 111-035-144) for 1 h at RT. Protein bands were detected on the ChemiDoc Imaging Systems (Bio-Rad) by adding Immobilon Forte Western HRP substrate (Cat. WBLUF0500). Band intensities were quantified with ImageJ and normalized to GAPDH.

Immunofluorescence

Cells were seeded on sterilized coverslips at a density of 50.000 cells per coverslip. Following 24hrs cells were treated with 5 µM olaparib (ThermoFisher Scientific, Cat. AC466290010) for 1 h at 37 ºC; then, UV irradiation was performed (0.4 J/cm^2 for MCF7 and 0.6 J/cm^2 for BT474) and cells incubated at 37 ºC for 1h. Cells were fixed with 4% formaldehyde for 15 min at RT, washed three times with TBS, permeabilized with 0.2% Triton X-100 for 10 min at RT, washed again three times with TBS, and subsequently blocked with 1% BSA in TBS for 1h at RT. Primary antibodies H3S28ph (1:400; Cell Signalling, Cat. 9713, and PAR/pADPr (1:100; R&D Systems, Cat. 4335-MC-100) were incubated overnight at 4 ºC in a humid chamber. The next day, after 3 washes with TBS, incubation with secondary antibodies was performed for 1 h at RT in the dark (anti-mouse IgG Alexa Fluor 488 (1:1000; ThermoFisher Scientific, Cat. A11001) and anti-rabbit IgG Alexa Fluor 568 (1:1000; ThermoFisher Scientific, Cat. A11011). The nuclei were stained when mounting the coverslips with Slowfade™ Gold Antifade Reagent with DAPI (Cat. S36938, ThermoFisher Scientific). Fluorescent images were acquired using confocal microscopy (Leica Microsystems, Cat. #DM6000), equipped with a 63X oil-immersion objective. DAPI was excited using a 405 nm laser, Alexa Fluor 488 with a 488 nm laser, and Alexa Fluor 568 with a 552 nm laser. Fluorescence intensity was quantified using ImageJ.

Cell proliferation assay

Cells were seeded in 96-well plates at a density of 20.000 cells per well and incubated on the IncuCyte® Live Cell Analysis System (Sartorius, USA). The day after, cells were treated with 5 μM olaparib (ThermoFisher Scientific, Cat. AC466290010) for 1 h; then, UV irradiation was performed (0.4 J/cm^2 for MCF7 and 0.6 J/cm^2 for BT474) and cell proliferation was monitored for 4 days in the IncuCyte® Live Cell Analysis System acquiring images every 8 hours.

Colony formation assay

Cells were treated with 5 μM olaparib (ThermoFisher Scientific, Cat. AC466290010) for 1 h; then, UV irradiation was performed (0.4 J/cm^2 for MCF7 and 0.6 J/cm^2 for BT474). After 1 h, cells were seeded in 6-well plates at densities of 250, 500 and 1000 cells per well and cultured for 15 or 30 days (MCF7 and BT474 cell line, respectively). Colonies were fixed and stained using 0.5% crystal violet diluted in methanol for 10 min at RT; then, several washes with H_2O were performed. Images were acquired with ChemiDoc Imaging Systems (Bio-Rad). Colony area in each condition was calculated by ImageJ.

Spheroids formation and viability assay

For spheroid formation assays, 2D-cultured cells were treated with 5 μM olaparib (ThermoFisher Scientific, Cat. AC466290010) for 1 h; then, UV irradiation was performed (0.4 J/cm^2 for MCF7 and 0.6 J/cm^2 for BT474). The day after, cells were plated at a density of 500 cells per well in 96-well “U” bottom plates (ThermoFisher Scientific, Cat. 332305) and incubated for 12 days to allow growth and spheroid formation. Spheroid viability was assessed using Invitrogen™ LIVE/DEAD™ Cell Imaging Kit (488/570) (ThermoFisher Scientific, Cat. R37601) following manufacturer's protocol. Spheroid size and fluorescence intensity were quantified using ImageJ.

Cell cycle assay

Cells were seeded at a density of 250.000 cells per well in 6-well plates. After 24 hours, cells were treated with 5 μM olaparib (ThermoFisher Scientific, Cat. AC466290010) for 1 h; then, UV irradiation was performed (0.4 J/cm^2 for MCF7 and 0.6 J/cm^2 for BT474). After 24 and 72 hours, cells were trypsinized and stained. Briefly, for each sample, the staining solution contained 10% Triton X-100, 10 mg/mL RNase A, 1 mg/mL propidium iodide, 20% FBS, and Phosphate Buffered Saline (PBS) to final volume. Data were acquired using a CytoFLEX S flow cytometer (Beckman Coulter), where propidium iodide was excited using a 488 nm laser and detected in the APC channel. Cell cycle distribution was analyzed using CytExpert software.

RNA extraction

Total RNA was extracted using NZY total RNA isolation kit (NZYtech, Cat. MB13402) following manufacturer’s instructions.

cDNA synthesis

cDNA was synthesized from 100 ng of RNA using the High Capacity cDNA Reverse Transcription kit (ThermoFisher Scientific, Cat. 4368814) following manufacturers' protocol. cDNA synthesis was carried out in the Bio-Rad T100™ Thermal Cycler using the following program: 25°C for 10 min, 37°C for 120 min, 85°C for 5 min and a final hold at 4°C.

Real-time qPCR

RT-qPCR was performed using the SYBR® Green qPCR Supermix (Bio-Rad, Cat. 1725272). For each reaction, 2 µL of primers, 10 µL SYBR Green and 6 µL of milliQ H_2O were mixed with 2 µL of cDNA. The qPCR was performed in the CFX96 real-time qPCR machine (Bio-Rad). GAPDH was used as the internal control gene, and relative gene expression levels were calculated using the 2^–ΔΔCT method. Primers are listed in Supplementary Table 1.

Chromatin immunoprecipitation (ChIP)

5 million BT474 cells were cultured in p150 mm plates. The day after, cells were treated with 5 µM olaparib (ThermoFisher Scientific, Cat. AC466290010) for 1 h at 37 ºC; then, UV irradiation was performed (0.6 J/cm^2) and cells incubated at 37 ºC for 1h. Cells were fixed at 80% confluency with 1.42% of formaldehyde for 15 min at RT; fixation quenching was performed with 125 mM Glycine for 5 min at RT. Cells were scrapped on ice with PBS + 1X Complete™ Protease Inhibitors Cocktail without EDTA (PICs) (Cat. 05056489001, Roche), collected by centrifugation (2.000 g for 5 min at 4 ºC) and washed twice with PBS + PICs. Cell pellets were resuspended in IP buffer (150 mM NaCl, 50 mM Tris-HCl (pH 7.5), 5 mM EDTA, NP-40 (0.5% vol/vol), and Triton X-100 (1.0% vol/vol)) containing PICs, and subsequently lysed with a type A pestle. Lysates were incubated on ice for 10 min and centrifuged at 1250 g for 3 min at 4 ºC. Pellets were resuspended in 600 µL of IP buffer + PICs and incubated on ice for 10 min; then, they were sonicated with a Bioruptor Pico (Diagenode) on high for 25 min (30 seconds on, 30 seconds off). After sonication, samples were centrifuged at 16.000 g for 10 min at 4 ºC, and the supernatant containing the sonicated chromatin was collected.

A total of 25 µL was removed for input preparation and chromatin quantification. Briefly, 175 µL of TE buffer (Tris-HCl 10 mM (pH 8.0) and EDTA 1 mM) and 1 µL RNase A (10 µg/µL) were mixed with the input chromatin. Samples were incubated at 37 ºC for 30 min, and 2 µL proteinase K (10 µg/µL) was added before they were incubated at 55 ºC for 30 min and at 80 ºC for 2 h. An equal volume of phenol:chloroform:isoamyl alcohol (25:24:1) was added, then samples were centrifuged at 14.000 rpm for 10 min at 4 ºC, and the aqueous phase was transferred to a new tube. Then, samples were precipitating overnight at -20 ºC with 1/10 volume of 3M NaAc (pH 5.2) and 3 volumes of 100% EtOH. The next day, samples were centrifuged (14.000 rpm for 30 min at 4 ºC), and the pellet was washed with 5 volumes 70% EtOH. After centrifugation at maximum speed for 15 min at 4 ºC, pellets were resuspended in 25 µL of TE buffer, and DNA concentration was measured at 260 nm using Nanodrop 2000 (ThermoFisher Scientific).

For immunoprecipitation, 10 µg of sonicated chromatin was incubated with 2 µg of H3S28ph antibody (Abcam, Cat. ab32388) or IgG (Diagenode, kch-504-250) overnight at 4 ºC. The precipitated chromatin was collected via magnetic beads (Dynabeads™ Protein G, ThermoFisher Scientific, Cat. 10004D) and eluted with a buffer containing 100 mM $NaHCO_3$ and 1% SDS. Eluted chromatin was incubated with 2 µL proteinase K (10 µg/µL) at 55 ºC for 30 min and at 80 ºC for 2 h. An equal volume of phenol:chloroform:isoamyl alcohol (25:24:1) was added, then samples were centrifuged at 14.000 rpm for 10 min at 4 ºC, and the aqueous phase was transferred to a new tube. Then, samples were precipitating overnight at -20 ºC with 1/10 volume of 3M NaAc (pH 5.2) and 3 volumes of 100% EtOH. The next day, samples were centrifuged (14.000 rpm for 30 min at 4 ºC), and the pellet was washed with 5 volumes 70% EtOH. After centrifugation at maximum speed for 15 min at 4 ºC, DNA was air-dried and resuspended in 150 µL of TE buffer. The primers used for ChIP-qPCR are listed in Supplementary Table 1 and represented as percentage of input.

-Galactosidase assay

To assess the presence of senescent cells, cells were seeded at a density of 50.000 cells per well in 12-well plates. After 24 hours, cells were treated with 5 µM olaparib (ThermoFisher Scientific, Cat. AC466290010) for 1 h; then, UV irradiation was performed (0.4 J/cm^2 for MCF7 and 0.6 J/cm^2 for BT474). After 1, 4 and 5 days, cells were stained with the -galactosidase Detection Kit (Abcam, Cat. ab65351) following manufacturer's protocol (overnight incubation). Images were acquired with an EVOS M5000 Imaging System (ThermoFisher Scientific, Cat. #AMF5000) and -galactosidase signal was quantified by ImageJ.

ChIP-seq data analysis

Significantly enriched H3S28ph regions [18] were subjected to functional annotation using the Genomic Regions Enrichment of Annotations Tool (GREAT) [19]. Genomic regions of H3S28ph enrichment were analyzed using default parameters, which assigns the input genomic regions to genes based on a basal regulatory domain extending 5 kb upstream and 1 kb downstream of the transcription start site (TSS), with extension up to 1 Mb to the nearest gene. GREAT was used to identify functional categories including Gene Ontology: Biological Process, Cellular Component, Molecular Function. Statistical significance was determined using a hypergeometric test, and multiple testing correction was applied to obtain False Discovery Rate (FDR) Q-values. Enriched terms were ranked according to their Hyper FDR Q-values.

Cohort of patients analysis

Overall survival (OS) analysis in HR^+ breast cancer patients was performed using the Kaplan–Meier Plotter database [20]. Patients were stratified into high- and low-expression groups according to the median expression level of the gene of interest, and survival curves were generated accordingly. Additional survival analyses, OS and progression-free survival (PFS), were performed using GEPIA3 [21] with default parameters unless otherwise specified.

Gene expression and clinical data from the GSE173839 cohort were obtained from the Gene Expression Omnibus database [22]. This dataset includes patients treated with chemotherapy (paclitaxel + doxorubicin + cyclophosphamide) in the control arm or with a combination of olaparib and durvalumab in the treatment arm. Only HR^+ patients were included in the analysis. Patients were stratified into high- and low-expression groups according to the median expression level of the genes of interest. The association between gene expression levels and pathological complete response (pCR) was subsequently evaluated in these groups.

Statistical analysis

Experiments were independently repeated at least three times for reliability. Statistical analyses were carried out using GraphPad Prism (v9.0). Student's t-test was used for two-group comparisons, and one-way or two-way ANOVA followed by appropriate post-hoc tests were applied for multiple comparisons. A p-value < 0.05 was considered statistically significant.

Results

DNA damage-induced H3S28 phosphorylation is enhanced upon PARP inhibition

Hormone receptor (HR) positive MCF7 and BT474 breast cancer cells demonstrate a rapid and dose dependent increase in H3S28 phosphorylation in response to DNA damage induced by UV radiation (Fig. 1A-E and S1A). This all-or-none phosphorylation of H3S28ph increases with an expected activation of PARP1 enzymatic activity clearly shown by the elevated nuclear PARlyation signal (Fig. 1A-C and 1E). Further analysis and in-detailed quantification of serine 28 phosphorylation levels revealed an interesting observation; that the statistically significant induction of H3S28ph upon DNA damage, was further enhanced in the presence of the PARP inhibitor, olaparib (PARPi) (Fig. 1A-C). However, fluorescence signal co-localization of H3S28ph and PAR significantly decreased upon PARPi (Fig. 1D). Controlling for the effectiveness of olaparib the quantification of PAR levels showed, as expected, a complete suppression following PARPi treatment (Fig. 1A-C and S1A).

Combined DNA damage and PARP inhibition impairs tumour growth through a persistent G1/S checkpoint arrest

To assess the phenotypic consequences of H3S28ph and the changes in the levels after DNA damage in the presence or absence of PARPi in breast cancer we carried out a series of functional assays. Firstly, cell proliferation was examined through the Incucyte® Live Cell Analysis System. PARPi treatment contributes to a higher proliferative ability of non-damaged cells; however, UV damage significantly impairs cells' proliferative capacity after 48h, with PARPi-treated cells maintaining slightly higher proliferative activity (Fig. 2A and S1B). Colony-formation assays revealed a higher number and larger colony formation when PARP1 is inhibited (BT474 *p*-value = 0.0424; MCF7 *p*-value = 0.0079) (Fig. 2B-C

and S1C-D); however, upon DNA damage, only MCF7 colonies presented an increased area when combined with PARPi (Fig. 2C and S1E). To further investigate whether the effects observed in 2D colony formation and proliferation assays could translate into a three-dimensional context, we next evaluated the spheroid-forming capacity of breast cancer cells. Spheroids treated with PARPi were significantly larger than control spheroids, and this difference was consistently maintained across all time points examined (Fig. 2D-E and S1F-G). Additionally, when spheroids were stained for live and dead cells, those treated with PARPi exhibited 2-fold increase in viable cells within the 3D structure (Fig. 1F and S1H), revealing a strong potential effect of PARPi in promoting tumour initiation capacity. Interestingly, UV-treated cells were unable to create 3D spheroids, regardless of PARPi treatment.

To determine whether the effect of PARP inhibition in these phenotypical assays arose from alterations in cell cycle, we performed a detailed analysis of cell cycle phases at multiple time points. Treatment with PARPi alone induced a moderate increase in the G2 population, consistent with its mechanism of action when replication-fork stress occurs (Fig. 2G and S1J). In contrast, 24h after UV irradiation, the S-phase fraction was considerably reduced accompanied by an accumulation of cells in G1 (p-value = 0.0132), an effect that became even more pronounced when DNA damage was combined with PARPi (p-value = 0.0002) (Figure S1I-J). Interestingly, 72h following DNA damage exposure, cells remained predominantly in G1 phase (p-value < 0.0001), with an almost complete loss of S-phase and a substantially diminished G2 population (Fig. 2G and S1K). The combination with PARPi accentuated this profile, suggesting a robust and sustained G1/S checkpoint arrest over time.

Serine 28 phosphorylation drives senescence-associated transcription upon DNA damage combined with PARP inhibition

To elucidate whether the increased tumour initiating capacity and cell cycle arrest observed upon combined DNA damage and PARP inhibition reflected an entry of breast cancer cells into a dormant-like state, we assessed the expression of senescence-associated markers. Consistent with our previous findings, the key cell cycle regulators p14 (*CDKN2A*), p15 (*CDKN2B*) and p16 (*CDKN2A*) were markedly upregulated when damage was combined with PARPi in BT474 cells (Fig. 3A-C). In parallel, FOXA1, a transcription factor critically involved in G1-S phase transition control, was also statistically significant increased (Fig. 3D). A similar pattern was observed in MCF7 cells, which exhibited upregulation of p14, p21, FOXA1 and GATA3 upon combination of DNA damage and PARPi (Figure S2A-H). Collectively, these findings indicate that the enhanced tumour initiating capacity induced by UV exposure in the presence of PARPi is tightly associated with the activation of essential cell cycle regulatory genes, including p14 and p16.

Nevertheless, to determine whether serine 28 phosphorylation contributes to the regulation of these genes, chromatin immunoprecipitation (ChIP) assays were performed. Interestingly, H3S28ph was strongly enriched at the promoter regions of p14, p15, p16 and FOXA1 genes following combined DNA

damage and PARPi conditions, showing at least six-fold increase compared to DNA damage alone (Fig. 3E-H). In contrast, H3S28ph levels at these promoters were negligible in untreated cells or in cells treated with PARPi alone (Figure S2I-L). These results support a model in which serine 28 phosphorylation is specifically induced upon DNA damage in the context of PARP inhibition, thereby contributing to the transcriptional regulation of key cell cycle genes.

To investigate whether cell cycle arrest and upregulation of cell cycle markers was translated into a senescent phenotype, β-galactosidase activity was assessed at 1, 4 and 5 days following DNA damage. From day 4 onwards, senescent cells became detectable by blue staining in response to DNA damage, either alone or in combination with PARPi (Fig. 3I and S2M). However, quantitative analysis revealed that the combination of UV and PARPi treatment significantly enhanced the β-galactosidase activity, indicating an increased proportion of senescent BT474 and MCF7 cells (Fig. 3J and S2N, respectively). Overall, these data highlight a potential role for histone H3 serine 28 phosphorylation in regulating senescence-associated transcriptional programs following DNA damage in the context of PARP1 inhibition.

To further support the role of H3S28ph in the regulation of senescence-associated transcriptional programs, we analyzed available ChIP-seq datasets from an independent system [18], where Aurora B kinase, which is the canonical kinase responsible for serine 28 phosphorylation, was genetically ablated in $CD34^{-}$ mouse resting B cells. As expected, loss of Aurora B resulted in a complete depletion of H3S28ph genome wide (Fig. 4A), confirming the dependency of this histone modification on Aurora B activity. To understand the biological processes associated with H3S28ph-enriched loci, we employed Genome Regions Enrichment Analysis Tool (GREAT) [19] (Table S2). Notably, among the top enriched Mouse Phenotypes, “abnormal cellular replicative senescence” emerged as one of the most significant categories (*p*-value = 1.10E-11) (Fig. 4B). A detailed analysis of the gene list within this class showed that classic CDK inhibitors such as Cdkn2a and Cdkn2b were not present (Fig. 4C) however, visualization of H3S28ph occupancy at specific genomic loci demonstrated a clear enrichment at the promoter region of Cdkn2b (p15) in wild-type cells, which was completely lost upon Aurora B knock-out (Fig. 4D, left panel). Similarly, other senescence-associated genes within the enriched category, such as Brca1 and Brca2, presented a strong H3S28ph enrichment at their promoter regions in wild-type conditions, which was robustly decreased following Aurora B depletion (Fig. 4D, middle and right panels). Overall, these data suggest that H3S28ph is broadly associated with the chromatin of genes involved in senescence-related pathways. Importantly, loss of H3S28ph enrichment at key regulatory loci suggests that this histone modification may play a direct role in facilitating the transcriptional activation of senescence-associated genes.

Serine 28 phosphorylation-associated genes stratify survival and therapy response in HR^{+} breast cancer patients

Our findings suggest that serine 28 phosphorylation upon DNA damage modulates PARP1 activity and promotes the transcriptional activation of cell-cycle regulatory genes, ultimately leading to the accumulation of senescent breast cancer cells. As therapy-induced senescence has been proposed as a cause of tumour recurrence, we next investigated whether components of this regulatory axis were associated with clinical outcome in breast cancer patients. To this end, survival analyses were performed using the Kaplan-Meier Plotter platform in hormone receptor-positive (HR^+) breast cancer patients. Expression levels of *RPS6KA5* (encoding MSK1, the kinase responsible for H3S28 phosphorylation), *CDKN2A* (p14/p16) and *CDKN2B* (p15) were evaluated. Interestingly, HR^+ patients receiving combined chemotherapy and hormonal therapy exhibited significantly worse OS when *RPS6KA5* expression was low (Fig. 4E), suggesting that reduced activity of H3S28 phosphorylation might be associated with poorer clinical outcomes following DNA-damaging treatments. Consistent with this observation, patients expressing low levels of *CDKN2A* also presented significantly reduced OS, although this association was only statistically significant in patients treated with hormonal therapy alone (Fig. 4F and S3A). In contrast, no significant survival differences were observed when patients were stratified according to *CDKN2B* expression levels (Figure S3B). Finally, we evaluated the prognostic value of the combined gene signature. Notably, patients presenting low expression of the entire signature exhibited significantly poorer OS compared with those with higher expression levels (Fig. 4G). Together, these results reveal a clinically relevant association between reduced expression of the H3S28 regulatory axis and adverse outcomes in HR^+ breast cancer patients.

To further validate these observations in an independent dataset, we next performed *in silico* survival analyses using the GEPIA3 platform. Consistent with our previous results, stratification based on the combined gene signature revealed that patients with lower expression levels have a reduced OS compared with those expressing higher levels of the gene signature (Fig. 4H). In contrast, no significant differences were observed in PFS when patients were stratified using the same gene set (Figure S3C).

Finally, we explored whether the expression of genes associated with serine 28 phosphorylation influence therapeutic response in an independent clinical cohort of HR^+ patients (GSE173839). In this study, patients received either a combination of chemotherapeutic agents (control arm) or a combination of olaparib and durvalumab (treated arm). Overall, the treated arm exhibits a higher proportion of pathologic complete response compared with the control group (Fig. 4I). In addition, stratification according to gene expression revealed that patients with low levels of *RPS6KA5*, *CDKN2A* and *CDKN2B* have improved response rates when treated with the olaparib combination compared to the control arm (Fig. 4J). These results suggest that inhibition of PARP1 in combination with immunotherapy may enhance therapeutic response, even in tumours where genes affected by H3S28 phosphorylation are downregulated.

Discussion

The present study identifies histone H3 serine 28 phosphorylation as a chromatin modification that is dynamically induced in response to DNA damage and further amplified upon PARP1 inhibition in HR^+ breast cancer cells. Our data support a model in which the MSK1–H3S28ph axis contributes to a transcriptional reprogramming program associated with senescence-like states, ultimately promoting cell survival under genotoxic stress and facilitating resistance to PARP inhibitors.

A central observation of this work is that combined UV-induced DNA damage and PARP inhibition enhance H3S28 phosphorylation levels. This is consistent with earlier studies demonstrating that H3S28ph is a stress-responsive histone mark regulated by MSKs, particularly MSK1 downstream of ERK and p38 MAPK signalling [15, 23–25]. In the context of DNA damage, chromatin modifications are critical for coordinating repair and transcriptional responses [26]. While PARP1 has been extensively characterized as a key regulator of chromatin conformation and DNA repair [27], our findings suggest that PARP inhibition may reinforce alternative chromatin states, such as H3S28ph, that enable adaptive transcriptional programs.

PARP1 is a multifunctional enzyme that acts far beyond its canonical role in DNA break repair. It catalyses the PARylation of core and linker histones and chromatin-associated proteins, promoting local chromatin relaxation, recruitment of DNA repair machinery and transcriptional activation [27, 28]. PARP1 also participates in wider chromatin and nuclear organization providing the substrates required for nuclear ATP synthesis by NUDT5 essential for chromatin remodelling and transcription activation in response to stimuli including DNA damage [12, 14]. In addition, PARP1 facilitates the resolution of R-loops to maintain transcriptional integrity, and the formation of phase-separated nuclear condensates that spatially coordinate DNA repair machinery [12, 29]. Given the known role of H3S28ph in displacing repressive complexes resulting in a more open chromatin state [30, 31] this increased phosphorylation may reflect an adaptive mechanism that allows cells to modulate transcription and survive genotoxic stress in the absence of PARP1 activity. Indeed, previous work has shown that histone modifications influence PARP1 recruitment and activity, and that chromatin states can modulate the extent of PARP1 trapping on DNA [32]. Together, these data point to an intricate interplay between PARP1 and histone phosphorylation in shaping chromatin responses to stress.

Mechanistically, we demonstrate that H3S28ph is enriched at the promoter regions of genes associated with cell cycle arrest and senescence, including *CDKN2A* (p14/p16) and *CDKN2B* (p15), as well as transcription factors such as FOXA1 and GATA3. These results are in agreement with previous reports indicating that H3S28 phosphorylation facilitates transcriptional activation by promoting Polycomb displacement and counteracting the repressive mark H3K27me3 [31]. In this context, H3S28ph may function as a chromatin switch that enables rapid transcriptional reprogramming in response to stress. Notably, the upregulation of CDK inhibitors such as p21 and increased β-galactosidase activity observed in our experiments suggest a senescence-like phenotype, which has a demonstrated dual role in cancer therapy [33, 34]. Therapy-induced senescence has been considered as a tumour-suppressive mechanism; however, accumulating evidence suggests that senescent cancer cells can persist in a dormant state and contribute to disease relapse through the acquisition of pro-survival and pro-

inflammatory features, known as the SASP [35–37]. Our findings support this paradigm by showing that PARPi-treated cells do not undergo complete cytotoxicity but exhibit growth arrest, cell cycle redistribution toward G1 phase and increased senescence markers. Importantly, the association between H3S28ph and transcription of senescence-related genes suggests that this chromatin modification may actively sustain the senescence program. In support of this model, the analysis of independent ChIP-seq datasets from Aurora B-deficient cells revealed a global loss of H3S28ph accompanied by a strong depletion of this mark at the promoter regions of multiple genes associated with senescence-related pathways such as Cdkn2b, Brca1 and Brca2. Importantly, these observations derive from a distinct experimental system and cellular context, thus, should be interpreted with caution when extrapolating to breast cancer models. The original study [18] was not performed in breast cancer cells and does not recapitulate the specific genomic and epigenetic landscape of HR^+ tumours. However, the consistent loss of H3S28ph upon Aurora B depletion, together with its enrichment at key regulatory loci, supports a conserved role for this modification in facilitating transcriptional activation of programs linked to senescence.

An intriguing aspect of our study is the implication of MSK1 as an upstream regulator of this process. MSK1 (encoded by *RPS6KA5*) has been linked to immediate early gene activation and chromatin remodelling in response to stress signals [38, 39]. Our clinical analyses highlight a context-dependent association between the MSK1–H3S28ph axis and patient outcomes in HR^+ breast cancer. Kaplan–Meier survival analyses revealed that low *RPS6KA5* expression, together with senescence-associated genes (*CDKN2A* and *CDKN2B*), results in worse OS in patients undergoing hormonal therapy and chemotherapy. Notably, the combined gene signature (*RPS6KA5* + *CDKN2A* + *CDKN2B*) provided a more robust separation of patient outcomes than individual genes, suggesting that coordinated activation of this transcriptional program may better represent tumour evolution and therapy response. In line with this, analysis of pCR indicates that higher *CDKN2B* (p15) expression is associated with reduced treatment efficacy, supporting the idea that activation of this axis may contribute to adaptive resistance mechanisms. Furthermore, PARP inhibitors, such as olaparib, have shown significant efficacy in BRCA-mutated and HR-deficient breast cancers [40]; however, resistance remains a major clinical challenge. Our data suggest that chromatin-mediated adaptive responses, including H3S28 phosphorylation, may contribute to this resistance independently of canonical HR repair mechanisms. Targeting MSK1 or associated signalling pathways could therefore represent a novel strategy to enhance PARPi efficacy. Additionally, the combination of PARPi with senolytic agents (compounds that selectively eliminate senescent cells) has emerged as a promising approach to prevent tumour recurrence [41].

Conclusions

In conclusion, this study identifies a novel chromatin-based mechanism of adaptive resistance to PARP inhibition in HR^+ breast cancer, focused on MSK1-mediated H3S28 phosphorylation and its role in promoting a senescence-associated survival program. These findings contribute to our understanding of the interplay between DNA damage signalling, chromatin dynamic and therapeutic response, and

highlight the potential of targeting epigenetic regulators to overcome resistance and improve clinical outcomes in breast cancer.

Abbreviations

ATCC
American type culture collection
ChIP
Chromatin immunoprecipitation
DDR
DNA Damage Response
FBS
Fetal bovine serum
FDR
False discovery rate
h
Hour
HR
Homologous recombination
HR+
Hormone receptor positive
H3S28ph
Histone H3 Serine 28 phosphorylation
min
Minutes
OS
Overall Survival
P/S
Penicillin/Streptomycin
PAR
Poly(ADP-ribose)
PARP1
Poly(ADP-ribose) polymerase 1
PARPi
PARP inhibitor
PBS
Phosphate Buffered Saline
PFS
Progression-Free Survival
PIC

Protease Inhibitor Cocktail
pCR
pathological Complete Response
RT
Room temperature
SASP
Senescence-Associated Secretory Phenotype
TSS
Transcription start site
UV
Ultraviolet

Declarations

Ethics approval and consent to participate

Not applicable

Consent for publication

All authors have given their consent for publication

Availability of data and materials

All data generated or analysed during this study are included in this published article and its supplementary information files.

Competing interests

The authors declare no competing interests

Funding

This work was supported by the Ramón y Cajal Fellowship (RYC2021-030923-I) funded by MCIN/AEI/10.13039/501100011033 awarded to RW and by the AIRC IG-2022 grant 27712 awarded to R.F.

Authors contributions

Experimental procedures; A.T.P, C.M.Mo, E.M, H.B, C.M.Mi, L.L.F. Experimental design; R.W., A.T.P, C.M.Mo. Manuscript preparation; R.W., C.M.Mo, A.T.P., R.F. Funding acquisition; R.W. R.F. All authors reviewed the manuscript.

Acknowledgements

We would like to thank all members of the Biomedical Science department for their support.

References

1. Telli ML, Litton JK, Beck JT, Jones JM, Andersen J, Mina LA, et al. Neoadjuvant talazoparib in patients with germline BRCA1/2 mutation-positive, early-stage triple-negative breast cancer: exploration of tumor BRCA mutational status. Breast Cancer. 2024;31:886–97.
2. Fasching PA, Schmatloch S, Hauke J, Rey J, Jackisch C, Klare P, et al. Neoadjuvant Paclitaxel/Olaparib in Comparison to Paclitaxel/Carboplatin in Patients with HER2-Negative Breast Cancer and HRD-Long-term Survival of the GeparOLA Study. Clin Cancer Res. 2025;31:1596–604.
3. Lema L, Pérez-García JM, Blanch S, Balmaña J, García-Sáenz JÁ, Vegas EF, et al. Niraparib Plus Aromatase Inhibitors for Hormone Receptor-Positive/HER2-Negative Advanced Breast Cancer with a Germline BRCA Mutation. Cancers (Basel). 2025;17.
4. Li H, Liu Z-Y, Wu N, Chen Y-C, Cheng Q, Wang J. PARP inhibitor resistance: the underlying mechanisms and clinical implications. Mol Cancer. 2020;19:107.
5. Zou Y, Zhang H, Chen P, Tang J, Yang S, Nicot C, et al. Clinical approaches to overcome PARP inhibitor resistance. Mol Cancer. 2025;24:156.
6. Kanev P-B, Varhoshkova S, Georgieva I, Lukarska M, Kirova D, Danovski G, et al. A unified mechanism for PARP inhibitor-induced PARP1 chromatin retention at DNA damage sites in living cells. Cell Rep. 2024;43:114234.
7. Wright RHG, Castellano G, Bonet J, Le Dily F, Font-Mateu J, Ballaré C, et al. CDK2-dependent activation of PARP-1 is required for hormonal gene regulation in breast cancer cells. Genes Dev. 2012;26:1972–83.
8. Huang P, Chen G, Jin W, Mao K, Wan H, He Y. Molecular mechanisms of parthanatos and its role in diverse diseases. Int J Mol Sci. 2022;23.
9. Pickup KE, Pardow F, Carbonell-Caballero J, Lioutas A, Villanueva-Cañas JL, Wright RHG, et al. Expression of oncogenic drivers in 3D cell culture depends on nuclear ATP synthesis by NUDT5. Cancers (Basel). 2019;11.
10. Laspata N, Kaur P, Mersaoui SY, Muoio D, Liu ZS, Bannister MH, et al. PARP1 associates with R-loops to promote their resolution and genome stability. Nucleic Acids Res. 2023;51:2215–37.
11. Krishnakumar R, Kraus WL. PARP-1 regulates chromatin structure and transcription through a KDM5B-dependent pathway. Mol Cell. 2010;39:736–49.
12. Wright RHG, Lioutas A, Le Dily F, Soronellas D, Pohl A, Bonet J, et al. ADP-ribose-derived nuclear ATP synthesis by NUDIX5 is required for chromatin remodeling. Science. 2016;352:1221–5.
13. Wright RHG, Le Dily F, Beato M. ATP, mg2+, nuclear phase separation, and genome accessibility. Trends Biochem Sci. 2019;44:565–74.
14. Qi H, Grace Wright RH, Beato M, Price BD. The ADP-ribose hydrolase NUDT5 is important for DNA repair. Cell Rep. 2022;41:111866.

15. Thomson S, Clayton AL, Hazzalin CA, Rose S, Barratt MJ, Mahadevan LC. The nucleosomal response associated with immediate-early gene induction is mediated via alternative MAP kinase cascades: MSK1 as a potential histone H3/HMG-14 kinase. EMBO J. 1999;18:4779–93.
16. Sawicka A, Hartl D, Goiser M, Pusch O, Stocsits RR, Tamir IM, et al. H3S28 phosphorylation is a hallmark of the transcriptional response to cellular stress. Genome Res. 2014;24:1808–20.
17. Culerrier R, Carraz M, Mann C, Djabali M. MSK1 triggers the expression of the INK4AB/ARF locus in oncogene-induced senescence. Mol Biol Cell. 2016;27:2726–34.
18. Frangini A, Sjöberg M, Roman-Trufero M, Dharmalingam G, Haberle V, Bartke T, et al. The aurora B kinase and the polycomb protein ring1B combine to regulate active promoters in quiescent lymphocytes. Mol Cell. 2013;51:647–61.
19. McLean CY, Bristor D, Hiller M, Clarke SL, Schaar BT, Lowe CB, et al. GREAT improves functional interpretation of cis-regulatory regions. Nat Biotechnol. 2010;28:495–501.
20. Győrffy B. Pharmacologically actionable transcriptomic signatures across immune infiltration subtypes in the KM-plotter breast cancer cohort. ATR. 2026.
21. Kang Y-J, Pan L, Liu Y, Rong Z, Liu J, Liu F. GEPIA3: Enhanced drug sensitivity and interaction network analysis for cancer research. Nucleic Acids Res. 2025;53:W283–90.
22. Clough E, Barrett T, Wilhite SE, Ledoux P, Evangelista C, Kim IF, et al. NCBI GEO: archive for gene expression and epigenomics data sets: 23-year update. Nucleic Acids Res. 2024;52:D138–44.
23. Deak M, Clifton AD, Lucocq LM, Alessi DR. Mitogen- and stress-activated protein kinase-1 (MSK1) is directly activated by MAPK and SAPK2/p38, and may mediate activation of CREB. EMBO J. 1998;17:4426–41.
24. Josefowicz SZ, Shimada M, Armache A, Li CH, Miller RM, Lin S, et al. Chromatin kinases act on transcription factors and histone tails in regulation of inducible transcription. Mol Cell. 2016;64:347–61.
25. Gawrzak S, Rinaldi L, Gregorio S, Arenas EJ, Salvador F, Urosevic J, et al. MSK1 regulates luminal cell differentiation and metastatic dormancy in ER+ breast cancer. Nat Cell Biol. 2018;20:211–21.
26. Stadler J, Richly H. Regulation of DNA repair mechanisms: how the chromatin environment regulates the DNA damage response. Int J Mol Sci. 2017;18.
27. Ray Chaudhuri A, Nussenzweig A. The multifaceted roles of PARP1 in DNA repair and chromatin remodelling. Nat Rev Mol Cell Biol. 2017;18:610–21.
28. Huang D, Kraus WL. The expanding universe of PARP1-mediated molecular and therapeutic mechanisms. Mol Cell. 2022;82:2315–34.
29. Hottiger MO, Hassa PO, Lüscher B, Schüler H, Koch-Nolte F. Toward a unified nomenclature for mammalian ADP-ribosyltransferases. Trends Biochem Sci. 2010;35:208–19.
30. Yung PYK, Stuetzer A, Fischle W, Martinez A-M, Cavalli G. Histone H3 Serine 28 Is Essential for Efficient Polycomb-Mediated Gene Repression in Drosophila. Cell Rep. 2015;11:1437–45.

31. Lau PNI, Cheung P. Histone code pathway involving H3 S28 phosphorylation and K27 acetylation activates transcription and antagonizes polycomb silencing. Proc Natl Acad Sci USA. 2011;108:2801–6.
32. Bonfiglio JJ, Fontana P, Zhang Q, Colby T, Gibbs-Seymour I, Atanassov I, et al. Serine ADP-Ribosylation Depends on HPF1. Mol Cell. 2017;65:932-940.e6.
33. Hernandez-Segura A, Nehme J, Demaria M. Hallmarks of cellular senescence. Trends Cell Biol. 2018;28:436–53.
34. Manousakis E, Moreta-Moraleda C, Miralles CM, Pujolà AT, Baccara H, Franquet LL, et al. CDKN1A/p21 Influences the Survival and Expansion of Breast Cancer Stem Cells after Oxidative Damage. OR. 2026;0:1–10.
35. Milanovic M, Fan DNY, Belenki D, Däbritz JHM, Zhao Z, Yu Y, et al. Senescence-associated reprogramming promotes cancer stemness. Nature. 2018;553:96–100.
36. Wiley CD, Campisi J. The metabolic roots of senescence: mechanisms and opportunities for intervention. Nat Metab. 2021;3:1290–301.
37. Coppé J-P, Desprez P-Y, Krtolica A, Campisi J. The senescence-associated secretory phenotype: the dark side of tumor suppression. Annu Rev Pathol. 2010;5:99–118.
38. Strelkov IS, Davie JR. Ser-10 phosphorylation of histone H3 and immediate early gene expression in oncogene-transformed mouse fibroblasts. Cancer Res. 2002;62:75–8.
39. Pérez-Cadahía B, Drobic B, Davie JR. Activation and function of immediate-early genes in the nervous system. Biochem Cell Biol. 2011;89:61–73.
40. Lord CJ, Ashworth A. PARP inhibitors: Synthetic lethality in the clinic. Science. 2017;355:1152–8.
41. Yosef R, Pilpel N, Tokarsky-Amiel R, Biran A, Ovadya Y, Cohen S, et al. Directed elimination of senescent cells by inhibition of BCL-W and BCL-XL. Nat Commun. 2016;7:11190.

Figures

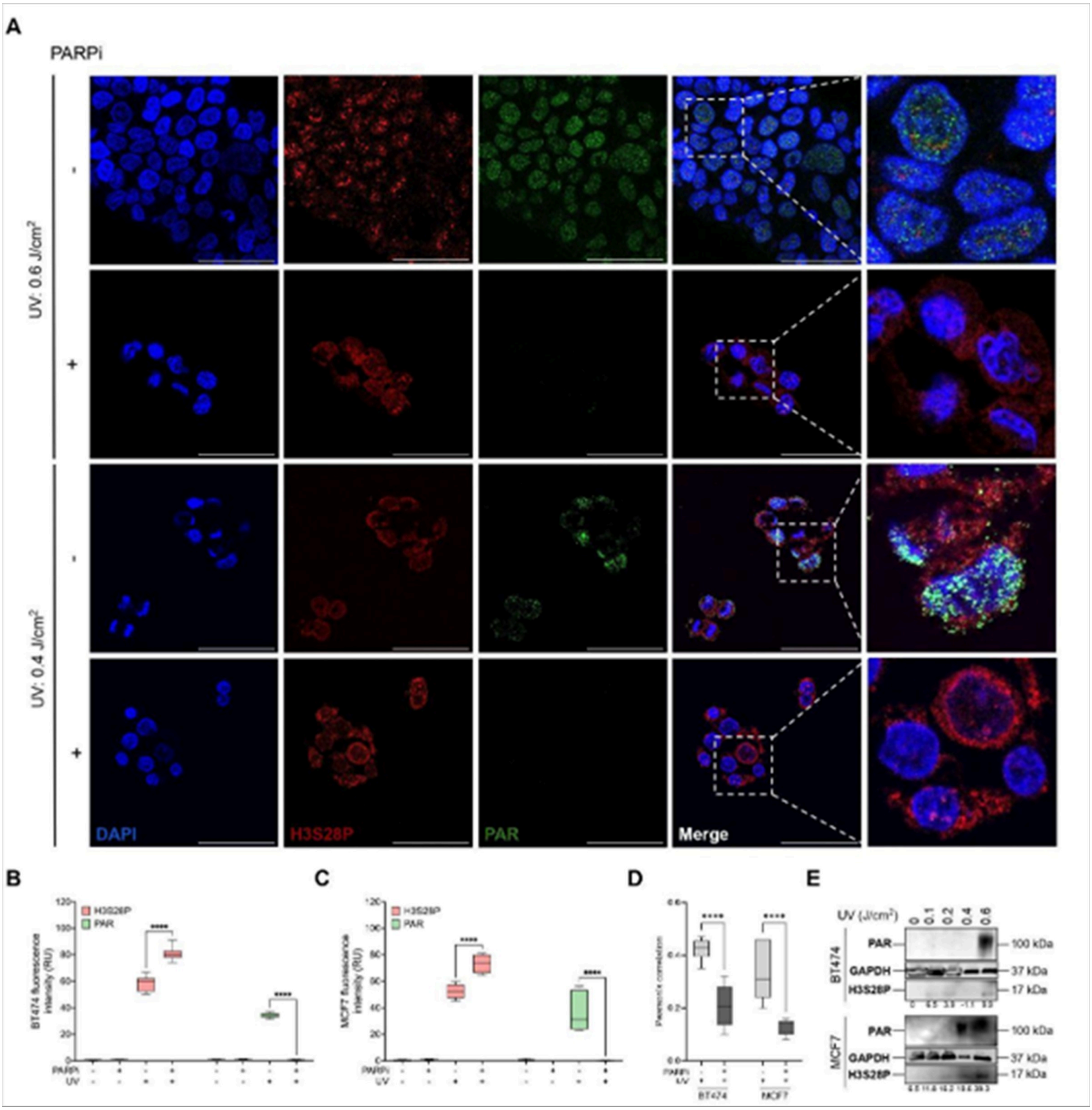


Figure 1

Combined UV damage and PARP inhibition enhance H3S28 phosphorylation. A. Representative immunofluorescence images showing serine 28 phosphorylation (red) and PAR (green) protein expression in cells treated with PARPi and exposed to UV irradiation (0.6 J/cm^2 for BT474 cell line and 0.4 J/cm^2 for MCF7 cell line). Nuclei were stained with DAPI (blue). Scale bar, 50 µm. **B-C.** Quantification of fluorescence intensity for serine 28 phosphorylation (red) and PAR (green) in BT474 (B) and MCF7 (C) cell lines under the indicated treatment conditions. Two-way ANOVA statistical analysis was performed

and p-values represented as **** (p <0.0001). **D.** Box plot representing the colocalization using Person's correlation coefficient between H3S28ph and PAR. Two-way ANOVA statistical analysis was performed and p-values represented as **** (p <0.0001). **E.** PAR and serine 28 phosphorylation protein levels detected by Western Blot in BT474 and MCF7 cell lines exposed to increasing doses of UV irradiation (0, 0.1, 0.2, 0.4 and 0.6 J/cm^2).

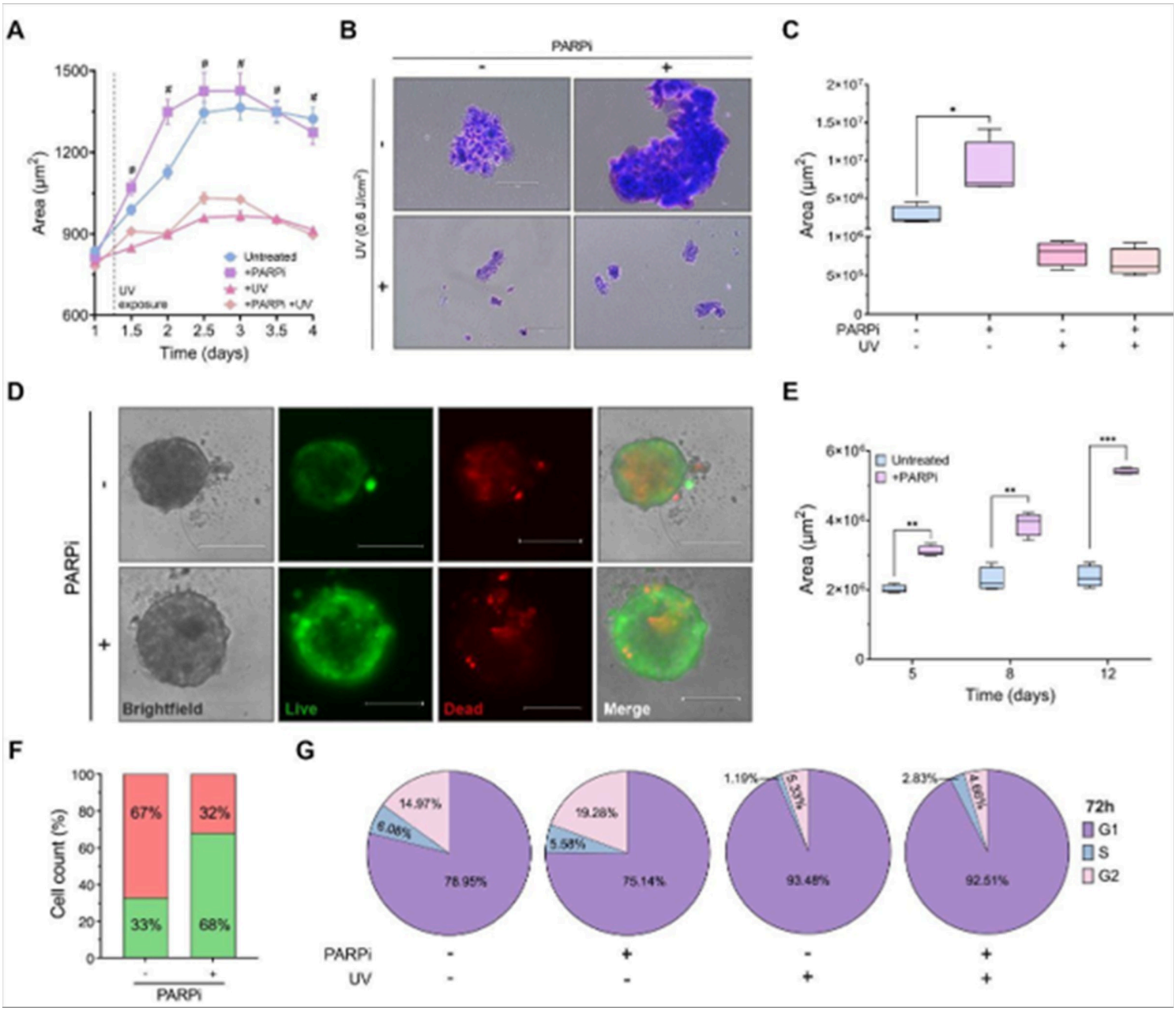


Figure 2

Combined UV damage and PARP inhibition suppress BT474 growth and induce G1/S arrest. A. Cell proliferation of BT474 cells monitored over time using the IncuCyte® Live Cell Analysis System following treatment with PARPi, UV irradiation or their combination. Two-way ANOVA statistical analysis was performed and significant differences between all groups were represented as # (p-value <0.0001) **B.** Representative colony formation images of BT474 cells under the indicated experimental conditions.

Scale bar, 150 μm. **C.** Box plot quantifying single-colony area under the indicated experimental conditions in BT474 cells. Statistical analysis was performed using Student's *t*-test and p-values represented as * ($p < 0.05$). **D.** Representative brightfield and fluorescence images of BT474 spheroids showing live (GFP, in green) and dead (RFP, red) cells following PARPi treatment. Scale bar, 150 μm. **E.** Box plot quantifying spheroid area in untreated and PARPi-treated BT474 cells over time. Statistical analysis was performed using Student's *t*-test and p-values represented as ** ($p < 0.005$) and *** ($p < 0.0005$). **F.** Bar graph showing the percentage of live (green) and dead (red) cells quantified from spheroids in panel D. **G.** Pie charts showing the distribution of BT474 cells across cell cycle phases (G0/G1, purple; S, blue; G2/M, pink) 72 h after treatment.

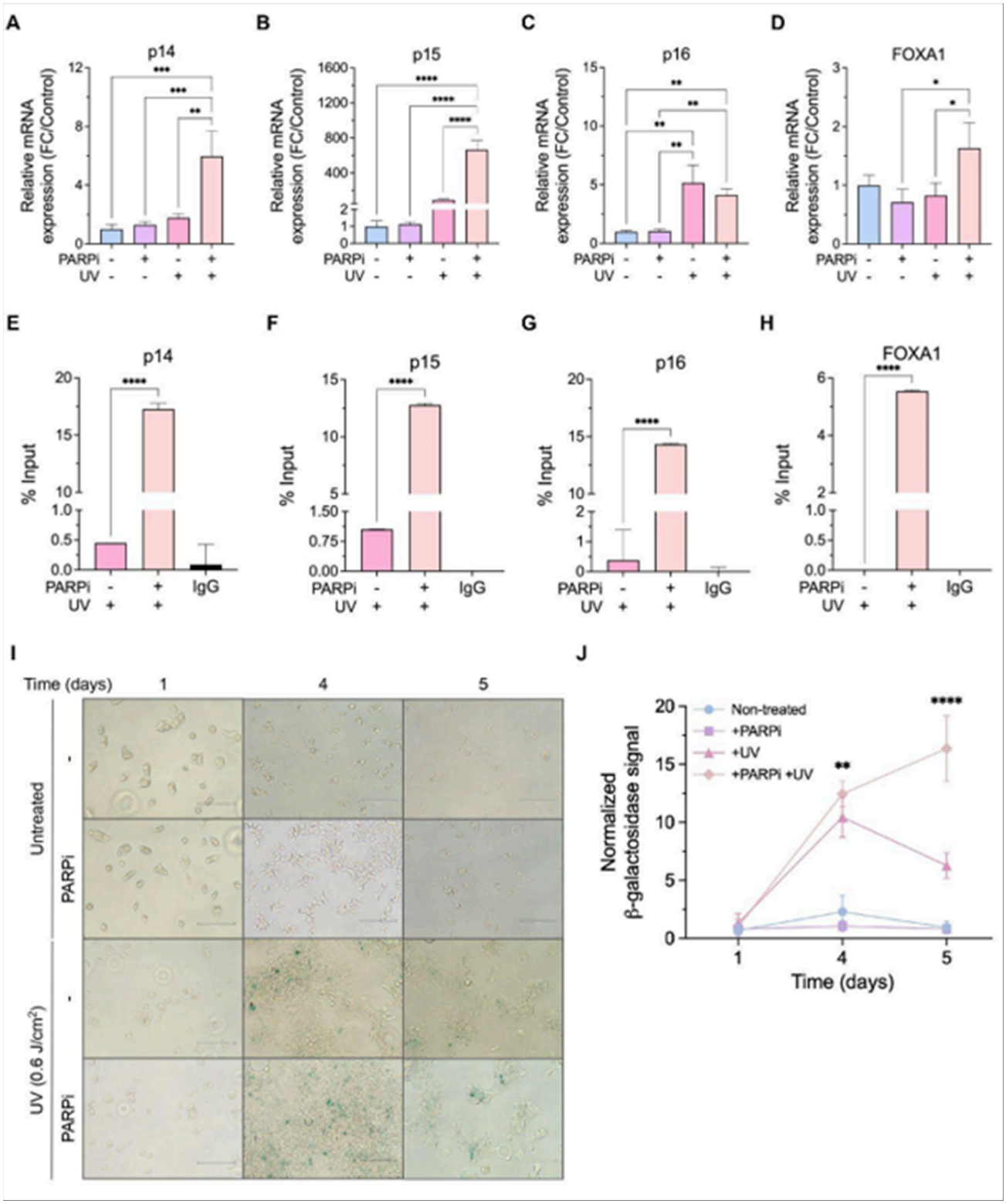


Figure 3

H3S28 phosphorylation promotes senescence-associated transcription upon UV damage and PARP inhibition. A-D. Relative mRNA expression of p14 (A), p15 (B), p16 (C) and FOXA1 (D) in BT474 cells under control, PARPi, UV (0.6 J/cm^2) or the combination of UV + PARPi treatments. Expression levels were normalized to GAPDH housekeeping gene. One-way ANOVA statistical analysis was performed and p-values represented as * ($p < 0.05$), ** ($p < 0.005$), *** ($p < 0.0005$) and **** ($p < 0.0001$). **E-H.** ChIP-qPCR

analysis of H3S28 phosphorylation enrichment at the promoter regions of p14 (E), p15 (F) p16 (G) and FOXA1 (H) in BT474 cells treated with UV or UV + PARPi. Data is presented as percentage of input chromatin. IgG immunoprecipitation was included as a negative control. One-way ANOVA statistical analysis was performed and p-values represented as **** ($p < 0.0001$). **I.** Representative brightfield images of BT474 cells under the indicated experimental conditions at different timepoints for β-galactosidase staining (blue) to assess senescence. Scale bar, 150 μm. **J.** Quantification of normalized β-galactosidase signal over time in BT474 cells under the indicated experimental conditions. Two-way ANOVA statistical analysis was performed and p-values represented as ** ($p < 0.005$) and **** ($p < 0.0001$).

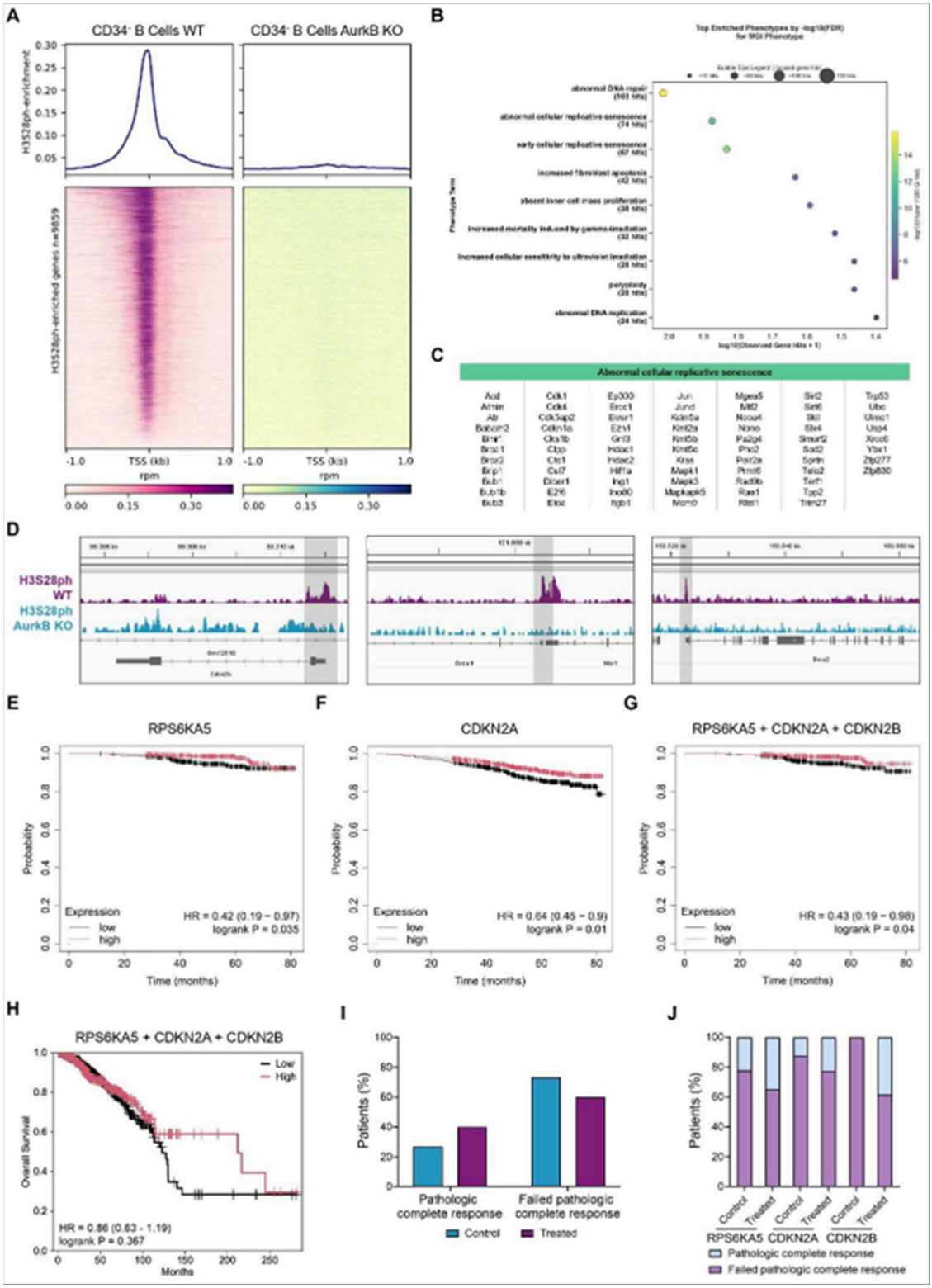


Figure 4

Serine 28 phosphorylation regulates senescence-associated genes and stratifies survival and therapy response in HR$^+$ breast cancer. A. Genome-wide distribution of H3S28ph ChIP-seq signal around transcription start sites (TSS) in wild-type (WT) and Aurora B knock-out (AurB KO) cells from an independent dataset [18]. Metagene profiles (top) and heatmaps (bottom) show a strong enrichment of H3S28ph at TSS regions in WT cells, which is depleted upon Aurora B depletion. **B.** Gene ontology

functional enrichment analysis of genes associated with H3S28ph peaks. Bubble plot representation of the top enriched Mouse Phenotype terms identified using GREAT [19]. Enrichment analysis was performed using default parameters, and terms are ranked according to the Hyper FDR Q-value. The x-axis represents the −log10(FDR Q-value), while bubble size indicates the number of genes associated with each term. **C.** Gene list corresponding to the “abnormal cellular replicative senescence” category (Figure 4B). **D.** Genome browser tracks showing H3S28ph enrichment (squared in grey) at representative senescence-associated gene loci in WT (purple) and AurB KO (blue) cells. Left panel: Cdkn2b; middle panel: Brca1; right panel Brca2. **E.** Kaplan-Meier OS curves for HR^+ breast cancer patients with low (black) or high (red) *RPS6KA5* (MSK1) expression treated with chemotherapy and hormone therapy. Survival curves were generated using the Kaplan-Meier Plotter. **F.** Kaplan-Meier OS curves for HR^+ breast cancer patients with low (black) or high (red) *CDKN2A* (p14/p16) expression treated with hormone therapy. Survival curves were generated using the Kaplan-Meier Plotter. **G.** Kaplan-Meier OS curves for HR^+ breast cancer patients stratified by low (black) or high (red) expression of the gene signature (*RPS6KA5* + *CDKN2A* + *CDKN2B*) treated with chemotherapy and hormone therapy. Curves were generated using the Kaplan-Meier Plotter. **H.** Kaplan-Meier OS curves for HR^+ breast cancer patients stratified by low (black) or high (red) expression of the same gene signature (*RPS6KA5* + *CDKN2A* + *CDKN2B*) generated using GEPIA3. **I.** Percentage of HR^+ breast cancer patients achieving pathological complete response (pCR) in the control (blue) and treatment (purple) arms of the GSE173839 cohort. **J.** Percentage of HR^+ breast cancer patients achieving pCR in the GSE173839 cohort stratified by low expression of *RPS6KA5*, *CDKN2A*, or *CDKN2B*.

Supplementary Files

This is a list of supplementary files associated with this preprint. Click to download.

- Graphicalabstract.docx
- SupplementaryFigures.docx